Automatic Recalibration of an Active Structured Light Vision System

Y. F. Li, *Senior Member, IEEE* and S. Y. Chen, *Member, IEEE*

***Abstract*— A structured light vision system using pattern projection is useful for robust reconstruction of 3D objects. One of the major tasks in using such a system is the calibration of the sensing system. This paper presents a new method by which a 2DOF structured light system can be automatically recalibrated, if and when the relative pose between the camera and the projector is changed. A distinct advantage of this method is that neither an accurately designed calibration device nor the prior knowledge of the motion of the camera or the scene is required. Several important cues for self-recalibration, including geometrical cue, illumination cue, and focus cue, are explored. The sensitivity analysis shows that high accuracy in depth value can be achieved with this calibration method. Some experimental results are presented to demonstrate the calibration technique.**

***Index Terms*--Structured light system, active vision, recalibration, pattern projection, 3D reconstruction.**

I. INTRODUCTION

SEVERAL methods have been explored for recovering the 3D information of an object or a scene, including stereovision, shape-from-motion, and active vision using structured light. Among them, the active vision approach has its advantages over others and has found successful applications in different areas including robotics. In many practical applications, the configuration of an active vision system needs to be changed on-line to achieve satisfactory measurements in which case it is desirable to be able to recalibrate the vision system without having to use special calibration apparatus as required by traditional calibration methods.

Most existing methods for calibrating active systems are based on static and manual calibration. During the calibration and 3D reconstruction, the vision sensor is usually placed at a fixed location. The calibration target (with specially made features, e.g. circles or squares) needs to be placed at several accurately known or measured positions in front of the sensor [1,2,3]. With a traditional method, the system must be calibrated again if the vision sensor is moved or the relative pose between the camera and the projector is changed. Frequent recalibrations in using such a system are tedious tasks.

Manuscript received February 28, 2002; revised August 31, 2002. This work was fully supported by the Research Grants Council of Hong Kong [Project No. CityU 1136/98E and CityU 1049/00E].

The authors are with the Department of Manufacturing Engineering and Engineering Management, City University of Hong Kong, Kowloon, Hong Kong (e-mail: meyfli@cityu.edu.hk, s.y.chen@plink.cityu.edu.hk).

Self-calibration of vision sensors is an attempt to overcome the above problem and it has been actively researched in recent years. However, most of the studies are concerned with passive vision including stereovision. For example, using the invariant properties of calibration matrix to motions, [4] proposed an optimization procedure for recalibration of a stereo vision sensor mounted on a robot arm. The technique for self-recalibration of varying internal and external parameters of a camera was explored in [5]. The issues in dynamic camera calibration were addressed in [6] to deal with unknown motions of the cameras and changes in focus. A method for automatic calibration of cameras was explored by tracking a set of world points [7]. Intensive efforts were also made in calibrating hand-eye systems including the use of self-calibration techniques [8,9,10]. Such self-calibration techniques normally require a sequence of images to be captured via moving the camera or the target [11], although with some special setup, two views can be sufficient for such calibration [12]. These methods cannot be applied directly to an active vision system which includes an illumination system using structured light in addition to the traditional vision sensor.

As for the calibration of active vision systems, most of the methods are based on static calibration and manual operations [13]. Similar to the calibration of passive stereo vision systems, attempts were made in calibrating a structured light system via transformation from 3D world coordinates to camera image plane coordinates using perspective transformation matrices [1,3]. To avoid using external calibrating devices and manual operations in the calibration, a self-reference method [14] was proposed. A set of points was projected to the scene and was detected by the camera to be used as reference in the calibration. With a cubic frame, Chu *et al*. proposed a calibration free approach for recovering unified world coordinates [15]. Fofi *et al*. discussed the problem in self-calibrating a structured light sensor [16]. A stratified reconstruction method based on Euclidean constraints by projection of a special light pattern was given. However, the work was based on the assumption that "projecting a square onto a planar surface, the more generic quadrilateral formed onto the surface is a parallelogram". This assumption is questionable. Consider an inclined plane placed in front of the camera or projector. Projecting a square on it forms an irregular quadrangle instead of parallelogram

as the two line segments will have different lengths on the image plane due to their different distances to the sensor. Jokinen's method [17] of self-calibration of light stripe systems is based on multiple views. The object needs to be moved by steps and several maps are required for the calibration. The registration and calibration parameters are obtained by matching the 3D maps via least errors. The limitation of this method is that it requires a special device to hold and move the object. A desktop approach to 3D shape reconstruction was proposed by Bouguet and Perona based on "weak structured lighting" [18]. This method provides an inexpensive solution to the problem, but the accuracy achievable in practical implementation is limited.

In this paper, we present our work in automatic calibration of our active vision system via a single view without using any special calibration device or target. Our interest falls in "self-calibration" and "self-recalibration" of active vision systems [19]. Here self-recalibration deals with situations where the system has been initially calibrated but needs to be calibrated again due to changed relative pose (the orientation and position) between the camera and projector. Self-calibration refers to cases where the system has never been calibrated and none of the sensor's parameters are known. Although the method described in this paper is mainly concerned with the former situation, it can also be applied to the latter case. In our work, some important cues are explored for the recalibration including the geometrical cue, focus cue, and illumination cue. The first two are used for the self-recalibration of a 2DOF system in the reported experiments. The illumination cue is not presented in detail here, but it is useful for improving accuracy or for systems with more degrees of freedom.

II. Self-Recalibration Task

The active vision system here consists of an LCD projector to cast a pattern of light onto the object and a camera to sense the light pattern as shown in Fig. 1. If a beam of light is cast, and viewed obliquely, the distortions in the beam line can be translated into height variations. To make the vision system adaptable to different objects/scenes to be sensed, we incorporated two degrees of freedom of relative motion in the system design, i.e. the orientation of the projector (or camera) and its horizontal displacement. The x-z plane is perpendicular to the plane of the projected laser stripe. The 3-D coordinate system is chosen based on the camera (or projector) center and its optic axis.

At the static calibration stage, the camera and the projector are calibrated to obtain the focal lengths (v_c, v_p) and the optical centers (x_{c0}, y_{c0}, x_{p0}). Once the perspective projection matrix of the camera and the equations of the planes containing the sheets of light relative to a global coordinate frame are given from the calibration, the triangulation for computing the 3D coordinates of object points simply involves finding the intersection of a ray from the camera and a plane from the projector.

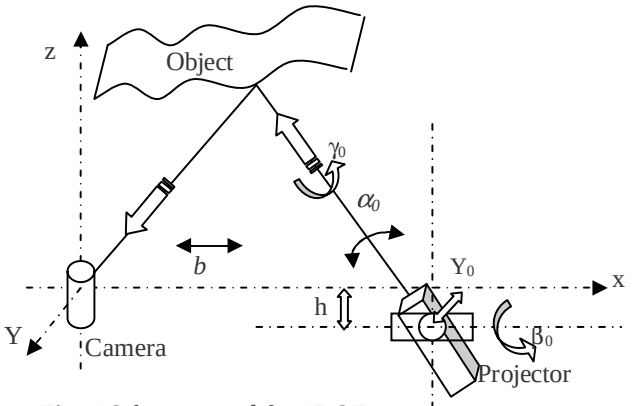

Fig. 1 Schematics of the 2DOF active vision system

The recalibration task is to determine the relative pose between the camera and the projector so that the 3D depth value can be computed by the triangulation principle. Now we firstly describe the 3D reconstruction in a general form.

For the camera, the relationship between the 3D coordinates of an object point based on the view of the camera $\mathbf{X}_c = [X_c \quad Y_c \quad Z_c \quad 1]^{\mathrm{T}}$ and its projection on the image $\mathbf{x}_c = [\lambda x_c \quad \lambda y_c \quad \lambda]^{\mathrm{T}}$ is given by

$$\mathbf{x}_c = \mathbf{P}_c \mathbf{X}_c , \tag{1}$$

where $\mathbf{P}_c$ is a 3×4 perspective matrix of the camera:

$$\mathbf{P}_c = \begin{bmatrix} v_x & k & x_{c0} & 0 \\ 0 & v_y & y_{c0} & 0 \\ 0 & 0 & 1 & 0 \end{bmatrix}_{3\times 4} . \tag{2}$$

Similarly, the projector is regarded as a pseudo-camera in that it casts an image rather than detects it. The relationship between the 3D coordinates of the object point from the view of the projector $\mathbf{X}_p = [X_p \quad Y_p \quad Z_p \quad 1]^{\mathrm{T}}$ and its back projection on the projector $\mathbf{x}_p = [\kappa x_p \quad \kappa]^{\mathrm{T}}$ is

$$\mathbf{x}_p = \mathbf{P}_p \mathbf{X}_p , \tag{3}$$

where $\mathbf{P}_p$ is a 2×4 perspective matrix:

$$\mathbf{P}_p = \begin{bmatrix} v_p & 0 & x_p^0 & 0 \\ 0 & 0 & 1 & 0 \end{bmatrix}_{2\times 4} . \tag{4}$$

The relationship between the camera view and the projector view is given by

$$\mathbf{X}_p = \mathbf{M}\mathbf{X}_c\ ,\ \mathbf{M} = \mathbf{R}_\theta\mathbf{R}_\alpha\mathbf{R}_\beta\mathbf{T} \qquad (5)$$

where $\mathbf{R}_\theta$, $\mathbf{R}_\alpha$, $\mathbf{R}_\beta$, and $\mathbf{T}$ are 4×4 matrices standing for the 3-axis rotations and a translation.

Substituting (5) into (3) gives

$$\mathbf{x}_p = \mathbf{P}_p\mathbf{M}\mathbf{X}_c\,. \qquad (6)$$

$$\text{Let } \mathbf{H} = \mathbf{P}_p\mathbf{M} = \begin{bmatrix}\mathbf{r}_1\\ \mathbf{r}_2\end{bmatrix}_{2\times 4}, \qquad (7)$$

where $\mathbf{r}_1$ and $\mathbf{r}_2$ are 4-dimensional row vectors. Equation (6) may be written as $\begin{bmatrix}\kappa x_p\\ \kappa\end{bmatrix} = \begin{bmatrix}\mathbf{r}_1\mathbf{X}_c\\ \mathbf{r}_2\mathbf{X}_c\end{bmatrix}$ from which we can derive

$$(x_p\mathbf{r}_2 - \mathbf{r}_1)\mathbf{X}_c = 0. \qquad (8)$$

Combining (1) and (8), we have

$$\begin{bmatrix}\mathbf{P}_c\\ x_p\mathbf{r}_2 - \mathbf{r}_1\end{bmatrix}\mathbf{X}_c = \begin{bmatrix}\mathbf{x}_c\\ 0\end{bmatrix}, \qquad (9)$$

$$\text{or } \mathbf{Q}\mathbf{X}_c = \mathbf{x}_{c+}\ , \qquad (10)$$

where $\begin{bmatrix}\mathbf{P}_c\\ x_p\mathbf{r}_2 - \mathbf{r}_1\end{bmatrix}\mathbf{X}_c = \begin{bmatrix}\mathbf{x}_c\\ 0\end{bmatrix}$ $\mathbf{Q}$ is a 4 by 4 matrix.

Then the world 3-dimensional position of a point on the object surface can be determined by

$$\mathbf{X}_c = \mathbf{Q}^{-1}\mathbf{x}_{c+}\,. \qquad (11)$$

From the above equations, the 3D object can be uniquely reconstructed if we know the matrix $\mathbf{Q}$ that contains 13 parameters from the two perspective matrices $\mathbf{P}_c$ and $\mathbf{P}_p$ and one coordinate transformation matrix $\mathbf{M}$. As the two perspective matrices can be determined at the static calibration stage, the dynamic recalibration task is to determine the relative $\mathbf{M}$ between the camera and the projector. There are 6 unknown parameters in (5), i.e.

$$\mathbf{u} = [\theta \quad \alpha \quad \beta \quad X_0 \quad Y_0 \quad Z_0]\,. \qquad (12)$$

Since the system considered in this paper has two degrees of freedom, only two of the six parameters are variable and the other four are constants which can be known from the static calibration. If the x-z plane is not perpendicular to the plane of the projected laser sheet, its angle Φ can also be identified at this stage. As the angle θ_0 =(90^o -Φ) is small and the image can be rectified by rotating the corresponding angle accordingly during the recalibration, we can assume that θ_0 = 0. The displacement in y-direction between the camera center and the projector center, Y_0, and the rotation angle β_0 are also small in practice. They do not affect the 3D reconstruction as the projected illumination consists only of vertical line stripes here. Therefore, we may assume that Y_0 = 0 and β_0 = 0. Thus, the unknown parameters are reduced to only two (α_0 and b) for the dynamic recalibration. Here h is a constant and α_0 and b have variable values depending on the system configuration.

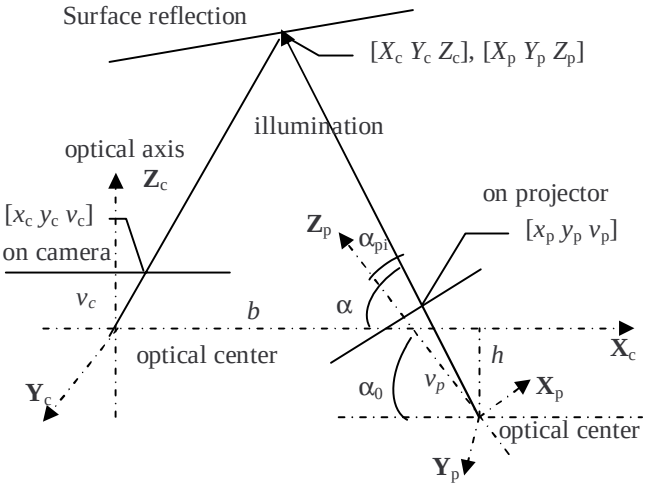

Fig. 2 Triangulation in the 2DOF system

For such a 2DOF system, the triangulation (9) for determining the 3D position of a point on the object surface is then simplified as (see Fig. 2)

$$[X_c\ Y_c\ Z_c] = \frac{b - h\cot(\alpha)}{v_c\cot(\alpha) + x_c}\ [\,x_c\ \ y_c\ \ v_c], \qquad (13)$$

where v_c is the distance between the camera sensor and the optical center of the lens, $\alpha = \alpha(i) = \alpha_0 + \alpha_p(i)$ is the projection angle, and

$$\alpha_p(i) = \tan^{-1}\left(\frac{x_p(i)}{v_p}\right), \qquad (14)$$

where i is the stripe index and $x_p(i)$ is the stripe coordinate on the projection plane: $x_p(i) = i \times$ stripe width + $x_p(0)$.

If the projector's rotational center is not at its optical center, h and b shall be replaced by:

$$h' = h - r_0\sin(\alpha_0) \text{ and } b' = b - r_0\cos(\alpha_0),$$

where r_0 is the distance between the rotational center and the optical center as illustrated in Fig. 3. Here, h and r_0 can be determined during the static calibration.

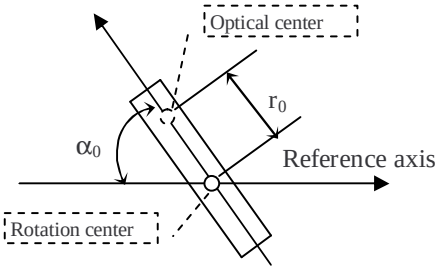

Fig. 3 The case when the rotational center is not at the optical center.

Since conventional self-calibration methods need several views to be acquired from different positions, they are inconvenient for the automated recalibration task here. Using a single view, it is in general difficult to determine all the unknown parameters in the calibration. Fortunately for the system here with 2DOF, self-recalibration can be achieved by utilizing the intrinsic cues. The use of geometrical cue and focus cue for determining the unknowns α_0 and b will be shown in the following sections.

III. Geometrical Cue

The geometrical cue describes the intrinsic relationship between the stripe locations on the camera and the projector. The geometrical constraint can be used to determine the unknown parameters of the vision system.

A. Geometrical constraint

Assume a straight line in the scene which is expressed in the camera coordinate system and projected on the X-Z plane:

$$Z_c = C_1 X_c + C_2 . \qquad (15)$$

The geometrical constraint between the projection and imaging of the scene line is obtained by substituting (13) into (15):

$$[\, b - h\cot(\alpha)\,]\,(v_c - C_1 x_c) - C_2\,[\, v_c \cot(\alpha) + x_c\,] = 0. \quad (16)$$

The parameters v_c, h, and v_p are constants that have been determined at the static calibration stage. $x_c = x_{ci} = x_c(i)$ and $\alpha_{pi} = \alpha_p(i)$ are known coordinates on the sensors. Therefore, α_0, b, C_1, and C_2 are the only four unknown constants and their relationship can be defined by three points.

Denote $A_0=\tan(\alpha_0)$ and $A_i=\tan(\alpha_{pi})$. The projection angle of an illumination stripe is

$$\cot(\alpha_0 + \alpha_{pi}) = \frac{1 - A_0 A_i}{A_0 + A_i} = \frac{v_p - A_0 x_p}{v_p A_0 + x_p}, \qquad (17)$$

where $x_p = x_p(i)$ is the stripe location on the projector's LCD and v_p is the distance between the LCD and the optical center. The x-coordinate value of the i^{th} stripe, $x_p(i)$, can be determined by (14). The stripe coordinate x_p and the projection angle α_{pi} are illustrated in Fig. 2.

Equation (16) can be written as,

$$(bA_0 - C_2 - h)v_c v_p + (hC_1 - bC_1A_0 - C_2A_0)v_p x_c + (b + A_0C_2 + hA_0)v_c x_p - (C_2 + bC_1 + hC_1A_0)x_c x_p = 0 \quad (18)$$

or $$x_c = W_1 + W_2 x_p + W_3(x_c x_p), \qquad (19)$$

where $W_1 = \frac{V_2V_3 - V_1V_4}{V_2V_4} - \frac{V_3}{V_4}$, $W_2 = -\frac{V_3}{V_2}$, $W_3 = \frac{V_2}{V_4}$, and

$$V_1 = bA_0 - C_2 - h, \qquad (20a)$$

$$V_2 = b + A_0C_2 + hA_0, \qquad (20b)$$

$$V_3 = hC_1 - bC_1A_0 - C_2A_0, \qquad (20c)$$

$$V_4 = C_2 + bC_1 + hC_1A_0 . \qquad (20d)$$

Equation (19) is the relationship between the stripe locations on the camera and the projector and is termed the geometrical constraint here.

B. Rectification of stripe locations

Within a view of the camera, there can be tens or hundreds of stripes from the scene. The stripes' coordinates (x_c, x_p) on the image and the projector should satisfy (19) in theory. In practice, however, the coordinates (x_c) obtained from the image processing may not satisfy this constraint, due to the existence of noise. To reduce the effect of noise and improve the calibration accuracy, the stripe locations on the image can be rectified by using a curve fitting method.

Let the projection error be

$$Q_{err}(W_1, W_2, W_3) = \sum_{i=1}^{m} [x_c'(i) - x_c(i)]^2 = \sum_{i=1}^{m} [W_1 + W_2 x_p + W_3(x_c x_p) - x_c]^2 \qquad (21)$$

Then W_1, W_2, and W_3 can be obtained by minimizing the projection error Q_{err} with respect to W_k :

$$\frac{\partial Q_{err}}{\partial W_k} = 0 , (k = 1, 2, 3). \qquad (22)$$

Using (21) in (22) gives

$$\begin{bmatrix} m & \sum_{i=1}^{m} x_p(i) & \sum_{i=1}^{m} x_c(i)x_p(i) \\ \sum_{i=1}^{m} x_p(i) & \sum_{i=1}^{m} x_p^2(i) & \sum_{i=1}^{m} x_c(i)x_p^2(i) \\ \sum_{i=1}^{m} x_c(i)x_p(i) & \sum_{i=1}^{m} x_c(i)x_p^2(i) & \sum_{i=1}^{m} x_c^2(i)x_p^2(i) \end{bmatrix} \begin{bmatrix} W_1 \\ W_2 \\ W_3 \end{bmatrix}$$

$$= \left[\sum_{i=1}^{m} x_c(i) \quad \sum_{i=1}^{m} x_p(i)x_c(i) \quad \sum_{i=1}^{m} x_p(i)x_c^2(i) \right]^{\mathrm{T}} \qquad (23)$$

or $\mathbf{GW} = \mathbf{X}$, $\mathbf{W} = \mathbf{G}^{-1}\mathbf{X}$. (24)

The stripe location in the camera coordinate is thus rectified as

$$x_c' = \frac{W_1 + W_2 x_p}{1 - W_3 x_p}. \qquad (25)$$

C. Solution using the geometrical cue

Equation (18) can be written as

$$v_c v_p V_1 + v_p x_c V_2 + v_c x_p V_3 - x_p x_c V_4 = 0. \qquad (26)$$

For an illumination pattern with n ($n \geq 3$) stripes on the image plane, Equation (26) can be expressed as

$$\begin{bmatrix} v_p v_c & v_c A_1 & v_p X_1 & -A_1 X_1 \\ v_p v_c & v_c A_2 & v_p X_2 & -A_2 X_2 \\ & \cdots & \cdots & \\ v_p v_c & v_c A_n & v_p X_n & -A_n X_n \end{bmatrix} \begin{bmatrix} V_1 \\ V_2 \\ V_3 \\ V_4 \end{bmatrix} = 0, \qquad (27)$$

or $\mathbf{A} \cdot \mathbf{V} = 0$, (28)

where $\mathbf{A}$ is an $n \times 4$ matrix, $X_i = x_c(i)$, $A_i = x_p(i)$, and $\mathbf{V}$ is a 4×1 vector. The following theorem is used for solving (27):

Theorem 1 (the rank of the matrix **A**). *Rank* (**A**) = 3.
Its proof is given in Appendix A.

Equation (27) has a solution in the form of

$$\mathbf{V} = k \, [\, v_1 \; v_2 \; v_3 \; v_4 \,]^{\mathrm{T}}, \; k \in \mathrm{R}, \qquad (29)$$

There exists an uncertain parameter k as the rank of matrix **A** is lower than its order by one. Using Singular Value Decomposition to solve the matrix equation (27) to find the least eigenvalue, we can obtain the optimal solution in the least square sense.

In a practical system setup, the z-axis displacement h is adjusted to 0 during a static calibration, and (29) gives a solution for the relative orientation: $A_0 = v_3/v_4$ and $\alpha_0 = \tan^{-1}(A_0)$. By setting $b = 1$ and solving (20) and (29), the 3D reconstruction can be performed to obtain an object shape (with relative size). If we need to obtain the absolute 3D geometry of the object, equation (29) is insufficient for determining the five unknowns, b, C_1, C_2, A_0, and k. To determine all these parameters, at least one more constraint equation is needed. The focus cue or the best-focused distance is used here for this purpose.

IV. Focus Cue

The focus cue is based on the fact that for a lens with a specified focal length the illumination pattern will be blurred on object surface unless it is projected on the best-focused distance. This gives another intrinsic constraint for the vision system in the self-recalibration.

A. Focus cue formulation

Fig. 4 shows the profile of a projection using synthetic illumination data. Fig. 4a is a typical illumination pattern on the LCD to be projected and its intensity profile is illustrated in Fig. 4b. Consider the straight line (15) in the scene (Fig. 4c). When the illumination pattern casts on such a line, the intensity distribution is nonlinear and is given by

$$I^i(x_l) = \frac{(z_0 + v_p)^2}{(z + v_p)^2 + (x_p + \frac{v_p}{z} x_p)^2} I_0, \qquad (30)$$

when $(-\frac{T}{2} < \frac{v_p}{z} x_p - 2nT < \frac{T}{2}), \mathrm{n} \in \mathrm{N}$. T is the stripe width of the source pattern.

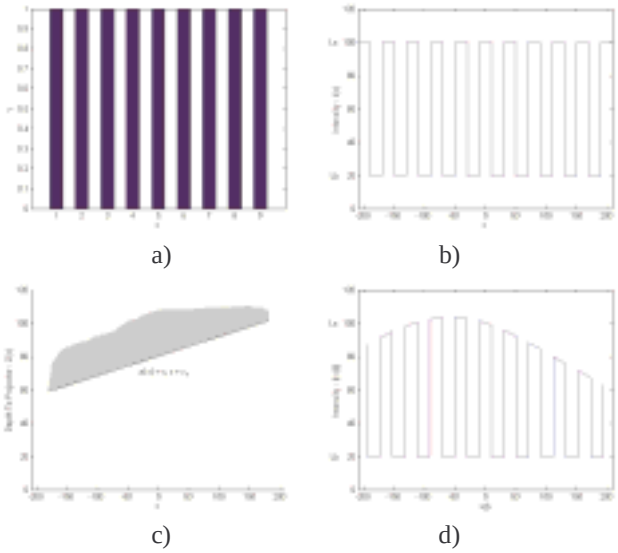

a) b) c) d)

a) A pattern of the projector's source illumination
b) The intensity distribution along a horizontal profile
c) A plane in the scene
d) The intensity profile on the surface (without blurring)

Fig. 4 Projection of illumination on the scene

Fig. 4d illustrates the curve (30) without considering the effect of blurring. However, the illumination is usually blurred unless it is projected on a plane at a special distance $z_0 = v_p f_p/(v_p - f_p)$. For all other locations in the scene, the

displacement will be

$$\Delta z = | z - z_0 | = | z - \frac{v_p f_p}{v_p - f_p} | . \quad (31)$$

The corresponding blur radius is proportional to Δz:

$$\sigma = \frac{v_p - f_p}{v_p F_{num}} \Delta z , \quad (32)$$

where $F_{num} = f_p / r$ is the f-number of the lens setting.

B. Determination of blur diameters

The blurring in the illumination is not evenly distributed in the blur circle. It can be described by a point spread function due to diffraction effects of light wave. A Gaussian model can be used to describe the blurring effect. For one dimensional case, the spread function is (Fig. 5a)

$$g_\sigma(x) = \frac{1}{\sqrt{2\pi}\sigma} e^{-\frac{x^2}{2\sigma^2}} . \quad (33)$$

The brightness of the scene illuminated by the projector is the convolution of the blur model with the ideal illumination intensity (30) (Fig.5b):

$$I(x_l) = I^i(x_l) \otimes g_\sigma(x_l) = \int_{-\infty}^{+\infty} I^i(u) g_\sigma(x_l - u) du . \quad (34)$$

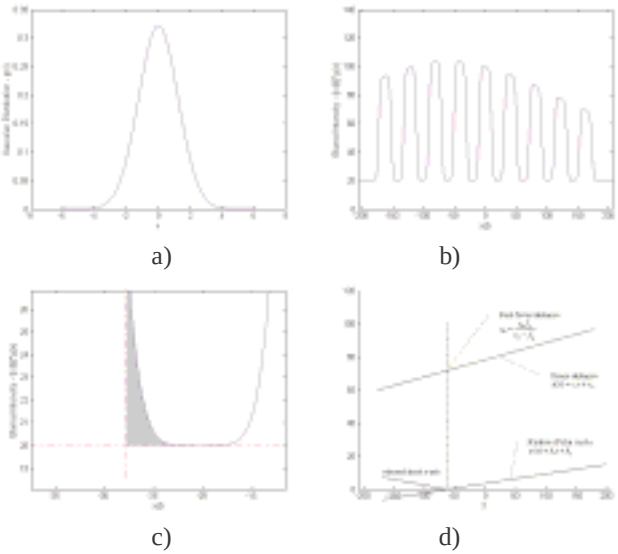

a) b) c) d)

a) Gaussian point spread function
b) Blur intensity distribution
c) The area for determining the blur diameter
d) Determination of the best-focused location

Fig. 5 Determination of blur diameters

The Fourier transform of (34) is

$$I_F(\omega) = {I_F}^i(\omega) G_\sigma(\omega) , \quad (35)$$

where $G_\sigma(\omega)$ is the Fourier transform of the Gaussian function

$$G_\sigma(\omega) = \int_{-\infty}^{+\infty} \frac{1}{\sqrt{2\pi}\sigma} e^{-\frac{x^2}{2\sigma^2}} e^{-jwx} dx = e^{-\frac{\sigma^2\omega^2}{2}} . \quad (36)$$

$I^i(x_l)$ can be approximated by averaging the intensity on a light stripe to simplify the Fourier transform, $I^i(x_l) = \bar{I}(x_l)$. If a coordinate system with its original at the center of the bright stripe is used, this value can be written as

$$\bar{I}(x) = \bar{I_0}[\varepsilon(x + \frac{T}{2}) - \varepsilon(x - \frac{T}{2})] , \quad (37)$$

where ε(.) is a unit step function.

The Fourier transform of (37) is

$${I_F}^i(\omega) = \bar{I_0} T \frac{\sin(\frac{\omega T}{2})}{\frac{\omega T}{2}} = \bar{I_0} T S_a(\frac{\omega T}{2}) , \quad (38)$$

Since $I(x_l)$ (the curve on the shaded area in Fig.5c) is measured by the camera, its Fourier transform $I_F(\omega)$ can be calculated. Rewriting (35) and integrating on both sides of it gives

$$\int e^{-\frac{\sigma^2\omega^2}{2}} d\omega = \bar{I_0} T \int \frac{I_F(\omega)}{S_a(\frac{\omega T}{2})} d\omega . \quad (39)$$

Since the left side is found to be

$$\frac{\sqrt{2}}{\sigma} \int_{-\infty}^{+\infty} e^{-(\frac{\sigma\omega}{\sqrt{2}})^2} d(\frac{\sigma\omega}{\sqrt{2}}) = \frac{\sqrt{2}\sqrt{\pi}}{\sigma} , \quad (40)$$

The blur radius can be computed by

$$\sigma = \frac{\sqrt{2\pi}}{\bar{I_0} T \int \frac{I_F(\omega)}{S_a(\frac{\omega T}{2})} d\omega} . \quad (41)$$

Neglecting the effect of blurring caused by multiple illumination stripes, we have the following theorem to determine the blur radius with a lower computational cost.

Theorem 2. When projecting a source illumination with a step profile, the blur radius is proportional to the area under the blurring curve:

$$\sigma = \frac{\sqrt{2\pi}}{I_0} S \,, \tag{42}$$

where I_0 is the intensity without considering the blurring and S is the area as illustrated in Fig.5c. The proof is given in Appendix B.

C. The best-focused location

With Theorem 2, by integrating the blur curve on each stripe edge, its blur radius can be calculated and a set of data are obtained. Since the blur diameters are unsigned, in order to obtain a straight line corresponding to the changing depth in the scene, we need to find the minimum value in the data set and separate the set into two parts. Their linear best-fits give two straight lines (Fig. 5d):

$$\sigma_l(x) = k_1 x + k_2 \text{ and } \sigma_r(x) = k_3 x + k_4 \,. \tag{43}$$

Finding the intersection of the left line and the right line gives

$$x_{best} = \frac{k_4 - k_2}{k_1 - k_3} \,, \tag{44}$$

which corresponds to $\Delta z = 0$ or $z = \frac{v_p f_p}{v_p - f_p}$ .On the image, $(x_{c,best}, y_{c,best})$ is the best-focused location.

D. Combination of the two cues

For the projector, the length of the light path is

$$\begin{aligned} l^2 &= (x-b)^2 + y^2 + (z+h)^2 \\ &= \frac{[bv_c + hx_c]^2 + [b\sin(\alpha) - h\cos(\alpha)]^2 y_c^{\,2}}{[v_c\cos(\alpha) + x_c\sin(\alpha)]^2} \,. \end{aligned} \tag{45}$$

At the best focused location, we have

$$\frac{v_p f_p}{v_p - f_p} = l_{best}\cos(\alpha - \alpha_0) \,. \tag{46}$$

or $\left[\frac{v_p f_p}{(v_p - f_p)\cos(\alpha - \alpha_0)}\right]^2 =$

$$\frac{[bv_c + hx_c]^2 + [b\sin(\alpha) - h\cos(\alpha)]^2 y_c^2}{[v_c\cos(\alpha) + x_c\sin(\alpha)]^2} \,, \tag{47}$$

Equation (47) is a constraint equation derived from the focus cue. Here h, v_p and f_p are known constants and b has appeared in the geometrical constraint. x_c, y_c, and α are replaced by the $x_{c,best}$, $y_{c,best}$. α_{best} determined in the above formulation. Thus together with the four equations in (29), there are 5 unknown parameters $\mathbf{S} = (k, b, C_1, C_2, \alpha_0)$ that can be found by solving the 5 equations. Using steepest descent approach which is an iterative method based on local gradients, we can obtain an accurate solution of the non-linear equation system. The algorithm for the self-recalibration is summarized as follows:

(1) Project the illumination patterns on the scene and capture the images from the camera. Find a line that is illuminated by at least three stripes.

(2) Compute the stripe locations in the image by a gradient operator and record their coordinates (x_{ci}, y_{ci}, i) with i being the stripe index.

(3) Calculate the geometrical cue **V** (29) based on the matrix equation (27).

(4) Determine the blur diameter for each stripe. Use linear fitting method to find the best-focused location (44).

(5) Combine the two cues, (29) and (47), to find the relative parameters.

(6) Obtain the matrices **H** (7) and **Q** (11) for performing 3D reconstruction.

V. Sensitivity Analysis

A. Recalibration Error

In this section, the sensitivity of the depth error to the recalibrated parameters (i.e. $\Delta\alpha_0$ and Δb) is analyzed. The relative reconstruction error of the scene depth is

$$\begin{aligned} E_z &= \frac{\Delta Z}{Z} = \frac{\partial Z}{\partial b}\frac{\Delta b}{Z} + \frac{\partial Z}{\partial \alpha_0}\frac{\Delta \alpha_0}{Z} \\ &= \frac{\Delta b}{b - h\cot(\alpha)} + \frac{(hx_c + bv_c)Z\Delta\alpha_0}{v_c[b - h\cot(\alpha)]^2\sin^2(\alpha)} \,. \end{aligned} \tag{48}$$

Now we consider the computational error of the stripe location on the captured image which can cause errors in the recalibrated parameters. We have

$$C_1 x_c + C_2 = \frac{bv_c - h\cot(\alpha)v_c}{v_c\cot(\alpha) + x_c} \tag{49}$$

$$\Delta\alpha_0 = -\left[\frac{2Z - C_2}{(h+Z)v_c} + \frac{C_1 bv_c - Z^2 + C_2 Z}{v_c(h+Z)^2}\right]\sin^2(\alpha)\Delta x_c \,. \tag{50}$$

Taking the derivative of (47) with respect to b and x_c gives

$$\begin{aligned} &(bv_c + hx_c)(v_c\Delta b + h\Delta x_c) + [b\sin(\alpha) - h\cos(\alpha)]y_c^2\sin(\alpha)\Delta b \\ &= \left(\frac{v_p f_p}{v_p - f_p}\right)^2[v_c\cos(\alpha) + x_c\sin(\alpha)]\sin(\alpha)\Delta x_c \end{aligned}$$

$$\Delta b = \frac{(\frac{v_p f_p}{v_p - f_p})^2 [v_c \cos(\alpha) + x_c \sin(\alpha)] \sin(\alpha) - bhv_c - h^2 x_c}{(bv_c + hx_c)v_c + [b\sin(\alpha) - h\cos(\alpha)]y_c^2 \sin(\alpha)} \Delta x_c$$

In the image processing, the stripe location error in the image can be given as

$$\Delta x_c = \frac{\delta}{\sqrt{12}}, \qquad (51)$$

where δ is the pixel width of the sensor. For a common CCD camera, δ is usually between 5μm and 20μm.

Consider a camera with a focal length v_c = 30mm and a sensor's pixel width δ = 11.6μm. If the projector is 0.5m away from the camera, it's orientation angle is 45°, h = 0 or $h << b$, and the object is at 1m distance from the camera, the relative orientation error is:

$$\frac{\Delta\alpha_0}{\alpha} = [1 - \frac{Z_0}{Z} + \frac{Z_b v_c + Z_0(Z - v_c)}{Z^2}] \frac{\sin^2(\alpha)}{v_c \alpha} \frac{\delta}{\sqrt{12}} \qquad (52)$$
$$\approx 0.00547\%.$$

The relative position error is:

$$\frac{\Delta b}{b} = \frac{(v_p f_p)^2}{v_c^2 \sec^2(\alpha) + y_c^2} \frac{v_c \delta}{bZ(v_p - f_p)^2 \sqrt{12}} \qquad (53)$$
$$\approx 0.0112\%$$

The relative depth error is:

$$E_z = \frac{\Delta b}{b - h\cot(\alpha)} + \frac{(hx_c + bv_c)Z\Delta\alpha_0}{v_c[b - h\cot(\alpha)]^2 \sin^2(\alpha)} \qquad (54)$$
$$\approx 0.0284\%.$$

By utilizing a large number of stripes in an image and employing a sub-pixel method in the image processing, the accuracy can be improved significantly. However, there exists noise resulting from the projector emission, surface reflection, and sensor perception. Static calibration errors are also passed on to the dynamic recalibration. These require a separate treatment in the analysis.

B. Error Propagations

The error propagation from initial static calibration to dynamic recalibration is analyzed in two steps. First, the static calibration error itself will cause depth error in the reconstruction. Second, the static calibration error can pass on to the dynamic recalibration and then to depth reconstruction. The static calibration is usually performed by placing a printed target in front of the sensor. The error resulting from this calibration stage will lead to 3D reconstruction errors directly and indirectly.

1) Errors directly caused by initial static calibration

The 3-D reconstruction error directly caused by initial static calibration error can be estimated by computing the partial derivative of (49). For example, assume that the camera focal length v_c has an amount of uncertainty Δv_c. This will give rise to a relative z-depth error

$$E_{z,v_c} = \left.\frac{\Delta Z}{Z}\right|_{v_c} = [1 - \frac{Z}{b\tan(\alpha) - h}] \frac{\Delta v_c}{v_c}. \qquad (55)$$

To prevent the static calibration error ($E_{vc} = \Delta v_c / v_c$) from being magnified or accumulated in the reconstruction, we need $|1 - \frac{Z}{b\tan(\alpha) - h}| \le 1$, i.e. $0 < Z \le 2b\tan(\alpha) - 2h$.

Ignoring the effect of small h and considering a case with 45° projection angle, we only need to ensure $Z \le 2b$. Hence to achieve satisfactory 3D reconstruction results, the object should be placed not farther than twice of the baseline distance. The influences of the uncertainties on the other parameters obtained from the initial calibration can be analyzed in a similar way and the resulting errors are found to be in the same order as the uncertainties.

2) Error propagation from static to dynamic calibration

The static calibration error will also cause dynamic calibration error, which in turn will cause 3D reconstruction error.

Among the initially calibrated system parameters (v_c, v_p, x_{c0}, and x_{p0}), we observed that the noise in v_c and x_{c0} has no influence on the results of α_0 and b. Hence, from the matrix equation (27), we only need to analyze the error propagation due to the noise in v_p and x_{p0}. However, the theoretical analysis is intractable here. In this research, we experimentally proved that the relative errors of both the recalibration parameters ($\Delta\alpha_0$ and Δb) are linear combinations of $\Delta v_p/v_p$ and $\Delta x_{p0}/x_{p0}$. Consider the above case with a similar assumption for the system configuration as in 1), we generated perfect data for the matrix **A** in (28), and fictitiously added the perturbations (Δv_p and Δx_{p0}) to it. The dynamic parameters (α_0 and b) were then computed. The two error surfaces against the perturbations in v_p and x_{p0}, were numerically found to be in the form

$$\frac{\Delta b}{b} = 1.1909 \frac{\Delta v_p}{v_p} - 0.1956 \frac{\Delta x_{p0}}{x_{p0}};$$
$$\frac{\Delta\alpha_0}{\alpha_0} = -0.6058 \frac{\Delta v_p}{v_p} - 0.1286 \frac{\Delta x_{p0}}{x_{p0}}.$$

The above dynamic calibration errors then will cause errors in the 3D reconstruction. The relative errors so caused can be determined quantitatively by (48).

In summary, the reconstruction errors can be traced to three sources: 1) directly from the static calibration; 2)

directly from the dynamic calibration; 3) indirectly from the static to dynamic calibration and to the final reconstruction. As the initial static calibration error will cause both direct and indirect reconstruction errors, special care needs to be exercised at this stage. In practice, however, the static calibration is normally performed off-line (before installed on the robot). Therefore, the parameters can be calibrated with a relatively high accuracy (usually between 0.001%-0.1%) [1,17,20]. This makes it possible to achieve high reconstruction accuracy with the dynamic recalibration approach. In our investigation, we found that an overall relative 3D reconstruction accuracy of about 0.03% is achievable (i.e. about 0.3mm error for an object at 1m from the camera).

VI. Experimental Study

The experimental setup is shown in Fig. 6. It consists of an LCD projector from ABW GmbH Ltd Co. and a PULNIX TMC-9700 camera with a CCD of 740 × 480 pixels and a 25mm lens. The projector is fixed whereas the camera can be moved vertically and rotated about the y-axis. The light stripe index is identified by a gray-encoded stripe projection method.

Fig. 6 The system setup

At the static calibration stage, the intrinsic parameters of the camera and the projector were obtained. Then at the dynamic recalibration stage, the illumination was projected onto a white background without predefined features. The camera's orientation and horizontal position were adjusted so that the camera could detect the illuminated area.

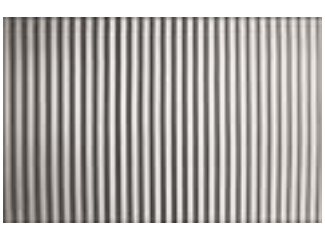

a)

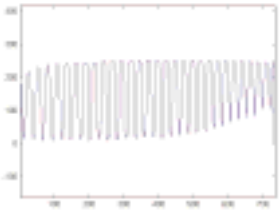

b)

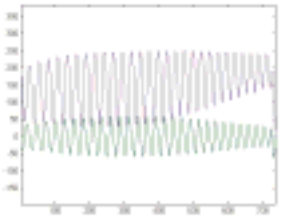

c)

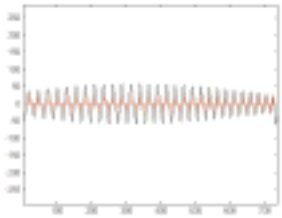

d)

a) The stripe illumination projected
b) An intensity profile on the image
c) Its derivative profile
d) The locations of stripe edges

Fig. 7 Determination of stripe locations

Fig.7a illustrates an image captured when the illumination was projected on the background wall. Fig. 7b shows an intensity profile and Fig. 7c shows its derivative profile. The stripe locations were determined by finding the peaks (Fig. 7d) of the derivative curve. Table 1 lists the results computed from the image, of the rectified stripe locations by (25), and blur radiuses by (42).

Table 1 Stripe locations and blur radiuses

Index ($i+i_0$)	Stripe locations (subpixel) (di[i])	Stripe distances (subpixel) di[i+1]-di[i]	Camera coord. $x_c(i)$	$x_c'(i)$ (rectified)	Blur radius (r[i])
1	15.6402		-4.1048	-4.1160	394.136
2	42.9004	27.260	-3.7886	-3.7921	341.153
3	70.7796	27.879	-3.4652	-3.4705	339.794
4	97.9553	27.175	-3.1499	-3.1512	314.350
5	124.980	27.024	-2.8364	-2.8342	266.668
6	152.085	27.105	-2.5220	-2.5194	241.496
7	178.884	26.799	-2.2111	-2.2068	196.548
8	205.751	26.866	-1.8995	-1.8965	207.838
9	231.917	26.165	-1.5960	-1.5883	153.154
10	258.089	26.172	-1.2924	-1.2823	148.398
11	284.109	26.020	-0.9905	-0.9784	115.748
12	310.702	26.593	-0.6820	-0.6766	156.415
13	336.678	25.975	-0.3807	-0.3769	171.202
14	362.160	25.481	-0.0851	-0.0793	227.485
15	387.994	25.834	0.2145	0.2163	240.614
16	413.648	25.653	0.5121	0.5099	291.551
17	438.915	25.267	0.8052	0.8015	363.936
18	464.515	25.600	1.1022	1.0910	490.529
19	489.102	24.586	1.3874	1.3787	526.596
20	513.822	24.719	1.6741	1.6643	570.515
21	538.055	24.234	1.9552	1.9481	578.125
22	562.455	24.399	2.2383	2.2299	614.716
...					

Using (27), the solution of the geometrical cue was found to be

$$k(v_1, v_2, v_3, v_4)=(-0.0973, 2.8569, -1.3123, 1.0).$$

For each stripe, the blur radius was determined by (42). The linear regression of these data gave two straight lines (Fig. 8)

$$R_1(x) = -1.0107\,x + 400.1845$$
$$R_2(x) = 1.6425\,x - 348.1617$$

The location of the minimum blur radius was determined by finding the intersection of the two lines $x_{0s} = 282.0507$.

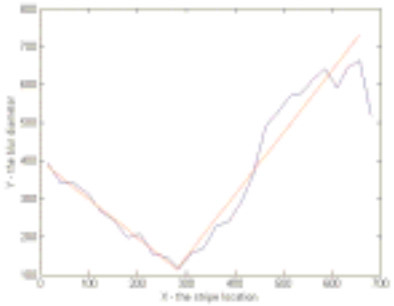

Fig. 8 Determination of the best focused location

The best-focused location on the camera coordinate system was thus

$$x_{c,\,best} = (x_{c0} - x_{0s})\,s_x = (369.5-282.05) \times 0.0116 = 1.0144.$$

$$y_{c,\,best} = (y_{c0} - y_{0s})\,s_y = (240-231) \times 0.0136 = 0.1224$$

$$i_{p,best} = \frac{(11-10)(282.0507-258.089)}{284.109-258.089} + 10 = 10.9209$$

$$x_{p,best} = (i_{p,best} + i_{p0})\,w_{stripe} = (10.921-21) \times 0.44 = -4.4522$$

$$\cot(\alpha_{best}) = \frac{v_p}{x_{p,best}} = \frac{91.2155}{-4.4522} = -20.4878$$

The two parameters for the relative pose were obtained by combining (29) and (47)

$$\alpha_0 = -37.3084^{o}, \text{ and } b = 588.9788\text{mm}.$$

On average, the above dynamic recalibration takes about 0.6 second in our implementation on a Pentium III-800 PC. The method is quite stable, with the steepest descent algorithm normally converging after no more than 10 iterations. Finally the relative matrices in (5), (7), and (10) were

$$\mathbf{M} = \mathbf{R}_\beta \mathbf{T} = \begin{bmatrix} 0.7954 & 0 & -0.6061 & -468.4647 \\ 0 & 1 & 0 & 0 \\ -0.6061 & 0 & 0.7954 & -356.9830 \\ 0 & 0 & 0 & 1 \end{bmatrix}.$$

$$\mathbf{H} = \mathbf{P}_p \mathbf{M} = \begin{bmatrix} 96.947 & 0 & -23.272 & -57100 \\ 0.6061 & 0 & 0.7954 & -356.98 \end{bmatrix}.$$

$$\mathbf{Q} = \begin{bmatrix} 30.089 & 0 & 0 & 96.947x_p - 0.6061 \\ 0 & 31.415 & 0 & 0 \\ 369.5 & 239.5 & 1 & -23.272x_p - 0.7954 \\ 0 & 0 & 0 & -57100x_p + 356.98 \end{bmatrix}^T.$$

The 3-D coordinates of a point on the object surface were recovered by

$$\mathbf{X}_c = \mathbf{Q}^{-1}\mathbf{x}_{c+}, \text{ for } x_p \in [-N, N].$$

With the above calibration results, an example for 3D object reconstruction was conducted. The reconstructed 3D surface of the object (a computer mouse) is shown in Fig. 9.

To test the dynamic performance of the method, we conducted another experiment using a precisely machined metal workpiece (shown in Fig. 10) as the object to be reconstructed. The workpiece was placed in front of the vision sensor at a distance of Z=388.5mm from the lens. We then arbitrarily changed the camera pose several times. The depth and width (D and L in Fig. 10) of the object were then measured following the dynamic recalibrations. Some typical results are listed in Table 2. At Pose 0, the results contain the reconstruction errors caused by the static calibration error only. Pose 1 and Pose 2 are two arbitrary sensor configurations. Our experiments showed that the 3D measurement errors using the dynamic calibration were about 1.5-3.0 times of those using static calibration only. In our multi-view dynamic experiments, no accumulative effect of the static calibration errors was observed. This is because the dynamic calibration is only relative to the initial pose (Pose 0). With our initial calibration technique currently implemented, we can achieve a dynamic accuracy of 0.015-0.3% in the scene depth measurements.

Such an achievable accuracy is considered quite satisfactory, since we did not make special attempts in improving the static calibration accuracy. The success in the dynamic recalibration and reconstruction can be attributed to the specialized device (the projector) adopted and the recalibration method developed in our work. This can be compared with the case when using a desktop system as in [18]. Although their application is for static only, the achievable accuracy is limited compared with our static calibration (in Pose 0). This is due to the errors that might be introduced in calibrating their table, light source, as well as the camera and in localizing the shadow edge of the stick.

This is the cost paid for the inexpensive hardware setup. An LCD projector is not a too expensive device. The benefit gained in employing such a specialized system will well justify its use in many applications where a stable accuracy is needed in the measurement and in particular when dynamic recalibration is desired.

Table 2 Experimental results in dynamic measurements

Pose	Feature	True value v0 (mm)	Measured value v (mm)	Relative error (Δv/V)	Relative error to scene depth (Δv/Z)
0	D	35	35.1623	0.00464	4.178×10^{-4}
0	L	55	55.2851	0.00518	7.388×10^{-4}
1	D	35	35.2588	0.00739	6.662×10^{-4}
1	L	55	55.4975	0.00905	0.001281
2	D	35	35.2756	0.00787	7.0940×10^{-4}
2	L	55	55.4231	0.00769	0.001089

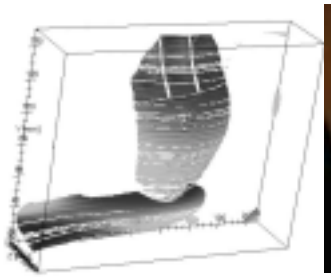

Fig. 9 The 3D object reconstructed

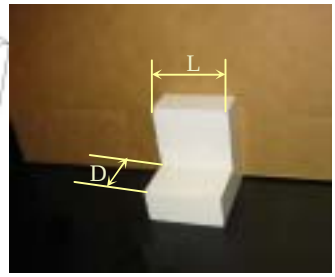

Fig. 10 The workpiece for dynamic test

VII. Conclusion

This paper presents our work in developing an active vision system which can be self-calibrated automatically. A recalibration method is developed that can be used in a dynamic application. The recalibration method does not require a special calibration target with pre-defined patterns or known motions of the sensor or the object. Whilst most previous self-calibration methods require multiple views at different positions, our method only needs to take a single view.

The intrinsic cues of the system have been explored for the self-recalibration. By taking advantage of the active sensing system, the geometrical cue and the focus cue have been successfully used in the calibration of the structured light vision system with 2DOF relative motion between the sensor and the illumination. The sensitivity analysis shows that with this method, a high accuracy in the depth measurement is achievable. This can be further improved if a good sub-pixel method and multi-stripe optimization techniques are employed.

Experiments were performed to apply the developed calibration method to a real vision system. The results show that using the dynamic recalibration, stable and accurate 3D reconstruction can be achieved. The illumination cue was not presented in this paper in treating the 2DOF system in use. Current work is going on in extending the method to the self-recalibration of a vision system with more motion degrees of freedom of motion and testing the dynamic performance using a robot work cell. Applications of the method will include advanced robotic applications where automated operations entail dynamically re-configurable sensing and automatic recalibration to be performed on-line without operator's interference.

Appendix A

Proof of Theorem 1. *Rank* (**A**) = 3.

Considering the 3×3 matrix $\mathbf{A}_{lt}$ in the left-top corner of the $n\times4$ matrix **A**. If $\det(\mathbf{A}_{lt}) \neq 0$, then $\text{rank}(\mathbf{A}) \geq 3$ is true.

$$\mathbf{A}_{lt} = \begin{bmatrix} v_p v_c & v_c A_1 & v_p X_1 \\ v_p v_c & v_c A_2 & v_p X_2 \\ v_p v_c & v_c A_3 & v_p X_3 \end{bmatrix}_{3\times3} \tag{A1}$$

With row operations, it can be transformed to

$$\mathbf{A}_{lt}' = \begin{bmatrix} v_p v_c & v_c A_1 & v_p X_1 \\ 0 & v_c(A_2 - A_1) & v_p X_2 - v_p X_1 \\ 0 & 0 & v_p(X_3 - X_1) - v_p(X_2 - X_1)\dfrac{A_3 - A_1}{A_2 - A_1} \end{bmatrix}. \tag{A2}$$

From (19) and (20), we have

$$U_2 = \frac{(V_2 V_3 - V_1 V_4)}{V_4^{\,2}} = \frac{v_c v_p (1 + A_0^2) C_2 (C_1 b + C_2 + h)}{(C_2 + bC_1 + hC_1 A_0)^2}. \tag{A3}$$

Suppose that the observed line does not pass through the optical center of either the camera or the projector, i.e.

$$C_2 \neq 0, \text{ and } C_1 b + C_2 + h = h - Z(0,b) \neq 0. \tag{A4}$$

$$\text{Hence} \quad U_2 \neq 0. \tag{A5}$$

For any pair of different light stripes illuminated by the projector, i.e. $A_i \neq A_j$, from (19),

$$X_i = U_1 + \frac{U_2}{U_3 + v_p A_i}, \tag{A6}$$

we have $X_i \neq X_j$, and

$$\mathbf{A}_{lt}'(1,1) = v_c v_p \neq 0, \tag{A7}$$

$$\mathbf{A}_{lt}'(2,2) = v_c(A_2 - A_1) \neq 0, \tag{A8}$$

$$\mathbf{A}_{lt}'(3,3) = v_p(X_3 - X_1) - v_p(X_2 - X_1)\frac{A_3 - A_1}{A_2 - A_1}$$
$$= \frac{v_p U_2 v_p^2 (A_1 - A_3)(A_2 - A_3)}{(U_3 + v_p A_1)(U_3 + v_p A_2)(U_3 + v_p A_3)} \neq 0. \quad \text{(A9)}$$

Hence, $rank(\mathbf{A}) \geq rank(\mathbf{A}_{lt}) = rank(\mathbf{A}_{lt}') = 3$.

On the other hand, rewrite matrix **A** using four column vectors, i.e.

$$\mathbf{A} = [c_{m1} \quad c_{m1} \quad c_{m1} \quad c_{m1}], \quad \text{(A10)}$$

where

$$c_{m1} = [v_p v_c \quad v_p v_c \quad \ldots \quad v_p v_c]^T, \quad \text{(A11)}$$
$$c_{m2} = [v_c A_1 \quad v_c A_2 \quad \ldots \quad v_c A_n]^T, \quad \text{(A12)}$$
$$c_{m3} = [v_p X_1 \quad v_p X_2 \quad \ldots \quad v_p X_n]^T, \quad \text{(A13)}$$
$$c_{m4} = [-X_1 A_1 \quad -X_2 A_2 \quad \ldots \quad -X_n A_n]^T. \quad \text{(A14)}$$

With the fourth column,

$$c_{m4} = \{-X_i A_i\} = \{-\frac{U_2 + U_1 U_3}{v_p} - U_1 A_i + \frac{U_3}{v_p} X_i\}$$
$$= \{\tau_1 v_c v_p + \tau_2 v_c A_i + \tau_3 v_p X_i\}$$
$$= \tau_1 c_{m1} + \tau_2 c_{m2} + \tau_3 c_{m3}. \quad \text{(A15)}$$

This means that the matrix's 4th column, c_{m4}, has a linear relationship with the first three columns, c_{m1} - c_{m3} . So the maximum rank of matrix **A** is 3, i.e. $rank(\mathbf{A}) \leq 3$.

Therefore we can conclude that

$$rank(\mathbf{A}) = 3. \quad \text{(A16)}$$

APPENDIX B

Proof of Theorem 2. The blur radius is proportional to the area under the blurring curve: $\sigma = \frac{\sqrt{2\pi}}{I_0} S$.

Consider the illumination whose intensity profile is a step function $I_0(x) = \begin{cases} I_0, & x < 0 \\ 0, & x \geq 0 \end{cases}$. The brightness on the illuminated scene is the convolution of Gaussian function and the source pattern:

$$I(x) = \int_{-\infty}^{+\infty} I_0(u) g(x-u) du = I_0 \int_{-\infty}^{0} \frac{1}{\sqrt{2\pi}\sigma} e^{-\frac{(x-u)^2}{2\sigma^2}} du \quad \text{(A17)}$$

$$= I_0 \int_{-\infty}^{0} \frac{1}{\sqrt{\pi}} e^{-(\frac{x-u}{\sqrt{2}\sigma})^2} d(\frac{x-u}{\sqrt{2}\sigma}) = \frac{I_0}{\sqrt{\pi}} \int_{\frac{x}{\sqrt{2}\sigma}}^{+\infty} e^{-y^2} dy. \quad \text{(A18)}$$

The size of the blurred area is the integration of the intensity profile function from 0 to +∞:

$$S = \int_0^{+\infty} I(x) dx = \frac{I_0}{\sqrt{\pi}} \int_0^{+\infty} \int_{\frac{x}{\sqrt{2}\sigma}}^{+\infty} e^{-y^2} dy dx \quad \text{(A19)}$$

$$= \frac{I_0}{\sqrt{\pi}} \int_0^{+\infty} \int_0^{\sqrt{2}\sigma y} e^{-x^2} dx dy = \frac{I_0}{\sqrt{\pi}} \int_0^{+\infty} \sqrt{2}\sigma y e^{-y^2} dy$$
$$= \frac{-I_0 \sigma}{\sqrt{2\pi}} \int_0^{+\infty} e^{-y^2} d(-y^2) = \frac{I_0 \sigma}{\sqrt{2\pi}}. \quad \text{(A20)}$$

That gives $\sigma = \frac{\sqrt{2\pi}}{I_0} S$. (A21)

REFERENCES

[1] D. Q. Huynh, "Calibration of a Structured Light System: A Projective Approach", *Proc. **IEEE** Conf. on Computer Vision and Pattern Recognition*, 1997, pp. 225 –230.

[2] F. W. DePiero and M. M. Trivedi, "3-D Computer Vision Using Structured Light: Design, Calibration and Implementation Issues", *Advances in Computers*, vol. 43, 1996, pp. 243-278.

[3] G. Sansoni, M. Carocci and R. Rodella, "Calibration and performance evaluation of a 3-D imaging sensor based on the projection of structured light", ***IEEE** Trans. on Instrumentation and Measurement*, vol. 49, no. 3, June 2000, pp. 628 -636

[4] J. Dias, A. de Almeida, H. Araújo and J. Batista, "Camera Recalibration with Hand-Eye Robotic System", *IECON 91*, Kobe, Japan, Oct. 1991.

[5] A. Zomet, L. Wolf and A. Shashua, "Omni-rig: linear self-recalibration of a rig with varying internal and external parameters", *Proc. Eighth **IEEE** Int. Conf. on Computer Vision*, vol. 1, 2001, pp. 135 -141.

[6] C. T. Huang and O. R. Mitchell, "Dynamic camera calibration", *Proc. Int. Symposium on Computer Vision*, 1995, pp. 169 -174.

[7] G. Wei; K. Arbter and G. Hirzinger, "Active self-calibration of robotic eyes and hand-eye relationships with model identification", ***IEEE** Trans. on Robotics and Automation*, vol. 14, no. 1, Feb. 1998, pp. 158 –166.

[8] S. D. Ma, "A self-calibration technique for active vision systems", ***IEEE** Trans. on Robotics and Automation*, vol. 12, no. 1, Feb. 1996, pp. 114 -120.

[9] M. Li, "Kinematic calibration of an active head-eye system", ***IEEE** Trans. on Robotics and Automation*, vol. 14, no. 1, Feb. 1998, pp. 153 -158.

[10] N. Andreff, R. Horaud, and B. Espiau, "Robot Hand-Eye Calibration using Structure from Motion", *Int. J. of Robotics Research*, vol. 20, no. 3, 2001, pp. 228-248.

[11] S. B. Kang, "Catadioptric self-calibration", *Proc. **IEEE** Conf. on Computer Vision and Pattern Recognition*, vol. 1, 2000, pp. 201 -207.

[12] Y. Seo and K. S. Hong, "Theory and practice on the self-calibration of a rotating and zooming camera from two views", ***IEE** proc. on Vision, Image and Signal Processing*, vol. 148, no. 3, June 2001, pp. 166-172.

[13] J. Batlle, E. Mouaddib and J. Salvi, "Recent Progress in Coded Structured Light as a Technique to Solve the Correspondence Problem: A Survey", *Pattern Recognition*, vol. 31, no. 7, July 1998, pp. 963-982.

[14] P. Hébert, "A Self-Referenced Hand-Held Range Sensor", *Proc. **IEEE** Third Int. Conf. on 3D Digital Imaging and Modeling*, Quebec City, Canada, May 2001, pp. 5-12.

[15] C. W. Chu, S. Hwang and S. K. Jung, "Calibration-free Approach to 3D Reconstruction Using Light Stripe Projections on a Cube Frame," Proc. ***IEEE** 3rd Int. Conf. on 3D Digital Imaging and Modeling*, Quebec City, Canada, June 2001, pp. 13-19.

[16] D. Fofi, J. Salvi and E. Mouaddib, "Uncalibrated Vision based on Structured Light", ***IEEE** Int. Conf. on Robotics and Automation*, Seoul, Korea, May 2001.

[17] O. Jokinen, "Self-calibration of a light striping system by matching multiple 3-D profile maps", ***IEEE** Proc. Second Int. Conf. on 3-D Digital Imaging and Modeling*, Ottawa, 1999, pp. 180-190.

[18] J. Y. Bouguet and P. Perona, "3D photography on your desk", *Proc. **IEEE** Int. Conf. on Computer Vision*, 1998, pp. 43-50.

[19] S. Y. Chen and Y. F. Li, "Self recalibration of a structured light vision system from a single view", *Proc. 2002 **IEEE** Int. Conf. on Robotics and Automation*, Washington DC, USA, May 2002, pp. 2539-2544.

[20] A. M. McIvor, "Nonlinear Calibration of a Laser Stripe Profiler", *Optical Engineering*, vol. 41, no. 1, 2002, pp. 205-212.